JOURNAL OF GUIDANCE, CONTROL, AND DYNAMICS
Vol. 19, No. 6, November–December 1996

Stability and Flying Qualities Robustness of a Dynamic Inversion Aircraft Control Law

Joseph S. Brinker* and Kevin A. Wise†
McDonnell Douglas Aerospace, St. Louis, Missouri 63166

Dynamic inversion, or feedback linearization theory, represents a commonly used nonlinear control method for designing aircraft control laws. This method has the ability to control a highly nonlinear plant but suffers from the lack of guaranteed robustness. The stability and flying qualities robustness of a dynamic inversion based control law, designed for a prototype aircraft, to uncertain aerodynamic parameters is analyzed. The results indicate that the pitch plane stability and flying qualities are robust to parameter uncertainties, but the lateral directional flying qualities are sensitive to uncertain stability derivatives.

Introduction

MANY evolving aircraft configurations present a considerable design challenge because of their utilization of innovative control effectors to increase maneuver capabilities and expand operational flight envelopes. Thrust vectoring, reaction control systems, pneumatic devices, and vortex control surfaces are commonly being used to augment conventional aerodynamic control surfaces. The design of flight control systems for these configurations, which meet stability and flying qualities requirements while fully realizing the performance capabilities of the vehicle, is complicated by both the number of control effectors and their highly nonlinear response characteristics.

Feedback linearization techniques[1,2] have received considerable attention in the literature regarding their application to the design of flight control systems for missiles and aircraft.[3–10] The basic idea of feedback linearization theory is that given a nonlinear plant

$$\dot{x} = f(x) + g(x)u \tag{1}$$

a control law that achieves the desired response characteristics may be formulated as

$$u = g(x)^{-1}[v - f(x)] \tag{2}$$

where v specifies the desired response. When the loops are closed using this control law, the resulting system is characterized by $\dot{x} = v$. General feedback linearization theory requires that the nonlinear plant be minimum phase since the resulting control law effectively inverts the plant and would otherwise produce a closed-loop system that is not internally stable.

The typical approaches for applying feedback linearization theory to the design of missile and aircraft control laws can be separated into two broad categories: those that consider the dynamics as a single coupled set of nonlinear differential equations and those that model the dynamics as evolving in multiple time scales. The multiple time scales approach typically separates the rotational (rotational rates) and translational (angle of attack, sideslip, and stability axis roll angle) dynamics by assuming that the rotational dynamics evolve much faster than the translational. This approach requires the assumption that the control effectors are primarily moment producing devices, which is reasonable for conventional aerodynamic control surfaces.

Several authors have applied feedback linearization theory in multiple time scales to the design of aircraft flight control systems.[3–6] Bugajski et al.[3] separate the dynamics into two time scales, where the fast dynamics consist of the vehicle rotational rates and the slow dynamics consist of angle of attack, sideslip, and stability axis roll angle. Application of dynamic inversion to the fast dynamics determines the control surface deflections (elevator, aileron, and rudder) required to generate the desired angular accelerations. Similarly, application of dynamic inversion to the slow dynamics specifies the rotational rates required to control the angle of attack, sideslip, and stability axis roll angle. Rotational acceleration commands for the fast loop dynamic inversion are determined from the rotational rate commands through designer specified desired dynamics. Similarly, rate commands to the slow loop dynamic inversion are determined from the pilot inputs via desired dynamics.

Snell et al.[4] extend this approach to an aircraft that has more control surfaces than dynamic quantities to control. The authors apply the two time scales dynamic inversion approach to the flight control design for a supermaneuverable aircraft whose control surfaces consist of aileron, rudder, canard, lateral axis thrust vector control (TVC), and pitch axis TVC. The fast dynamics are characterized by a nonsquare control distribution matrix [$g(x)$ in Eq. (1)] since there are five effectors available to generate the three desired rotational accelerations. Equation (1) thus represents an underdetermined set of equations. Since $g(x)$ is right invertible, the required control deflections may still be generated by Eq. (2).

The application of feedback linearization theory to aircraft flight control design has been formalized in Ref. 7.

Feedback linearization techniques have also been widely applied to augment linear design approaches. Wise et al.[8] used dynamic inversion to augment a linear quadratic based aircraft control law design by canceling the gyroscopic nonlinearities in the rotational dynamics. Feedback linearization techniques have also been used in conjunction with structured singular value (SSV) μ synthesis to address nonlinearity and robustness problems experienced in aircraft flight control at extreme operating conditions.[9,10]

There are two major concerns with developing nonlinear aircraft control laws using feedback linearization theory (or any nonlinear control design method). The first concern is with the lack of analysis tests to evaluate the robustness properties of the design. The second concern is with redesigning the control laws once a robustness problem has been identified. This paper focuses on developing/applying analysis tests for aircraft control laws designed using feedback linearization.

The problem of redesigning the control laws once a robustness problem has been identified is a very difficult and computationally intensive problem. For linear systems, Safonov et al.[11] and Goh et al.[12] have studied robust control system design using bilinear matrix inequalities. Software for solving these difficult problems is not readily available. For nonlinear systems this remains an open research topic.

Linear control systems are supported by an array of analysis methods that ensure the integrity of the design. These include stability

Received Nov. 7, 1995; revision received May 1, 1996; accepted for publication June 24, 1996.

*Senior Project Engineer, Advanced Systems and Technology—Phantom Works Division, Mail Code 1067126, P.O. Box 516.

†Senior Principal Technical Specialist, Advanced Systems and Technology—Phantom Works Division, Mail Code 1067126, P.O. Box 516. Senior Member AIAA.

margin measures, linear transient response evaluations, and stability and performance robustness tests. Analogous tools currently do not exist for nonlinear control laws but are under development.[13–17] Although researchers have made some progress toward the development of these nonlinear analysis tools,[16,17] the performance of nonlinear control laws is typically evaluated in industry by linearizing the system around a trim point and applying linear analysis methods.[18,19] This is the approach employed here.

This paper presents an evaluation of the stability and flying qualities robustness of a dynamic inversion based flight control law designed for a prototype aircraft. Robustness to aerodynamic parameter uncertainties is evaluated at the extremes of the operational flight envelope. Robust stability is evaluated using the deGaston–Safonov real multiloop stability margin.[20] SSV μ (Ref. 21) analysis is used to evaluate flying qualities robustness using the performance weighting filter proposed by Anderson.[22]

Control Law Design

The prototype aircraft control law investigated in this paper was designed by applying feedback linearization theory in two time scales. The vehicle's nonlinear dynamics used in the design are thoroughly documented in the literature.[23–25] The resulting control law structure is shown in Fig. 1. The stick logic generates angle of attack, stability axis roll rate, and sideslip commands based on the pilot stick inputs and is classically tuned to meet flying qualities objectives. Feedback linearization is then applied to generate the effective elevator, aileron, and rudder commands required to produce the desired responses to the stick inputs. The propulsion system forces and moments are driven by the throttle setting controlled by the pilot and thus are not treated as command inputs to be generated by the feedback linearization controller. A surface mixer, designed via an a priori control effector optimization, is used to generate individual control effector commands from the effective surface commands.

Control laws based on feedback linearization theory transform a nonlinear system into a linear system via nonlinear feedback control and a transformation of the state vector. Once the nonlinear system is linearized, linear control methods may be employed to design loop shapes that result in the desired response characteristics. In this paper, feedback linearization theory is used to develop a control law for a prototype aircraft through the solution of the noninteracting controls problem.[1] The solution of the noninteracting controls problem produces a controller that completely decouples the system into independent control channels, where a given output is only influenced by its corresponding input. This type of controller directly supports the flying qualities objectives of providing decoupled responses in the longitudinal, lateral, and directional axes.

The feedback linearization controller is derived by placing the dynamics of each time scale in the form of Eq. (1). In the fast time scale, the states are the stability axis rotational rates,

$$\boldsymbol{x} = [\,p_s \quad q \quad r_s\,]^T \tag{3}$$

and the control variables are the effective aileron, elevator, and rudder surface deflections,

$$\boldsymbol{u} = [\,\delta_a \quad \delta_b \quad \delta_r\,]^T \tag{4}$$

The objective of feedback linearization in the fast time scale is to use the surface deflections to control the rotational rates, and thus the outputs are chosen as

$$\boldsymbol{y} = \boldsymbol{x} = [\,p_s \quad q \quad r_s\,]^T \tag{5}$$

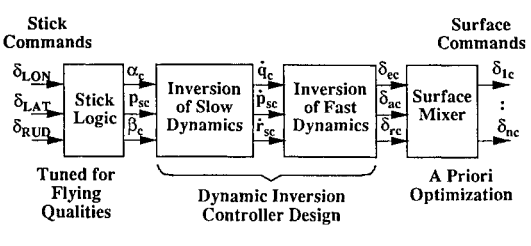

Fig. 1 Control law structure.

The dynamics governing this time scale can be expressed as

$$\begin{bmatrix} \dot{p}_s \\ \dot{q} \\ \dot{r}_s \end{bmatrix} = \begin{bmatrix} f_1(\boldsymbol{x}) \\ f_2(\boldsymbol{x}) \\ f_3(\boldsymbol{x}) \end{bmatrix} + \begin{bmatrix} \bar{L}_{\delta_a} & 0 & \bar{L}_{\delta_r} \\ 0 & M_{\delta_e} & 0 \\ \bar{N}_{\delta_a} & 0 & \bar{N}_{\delta_r} \end{bmatrix} \begin{bmatrix} \delta_a \\ \delta_e \\ \delta_r \end{bmatrix}$$

$$= f(\boldsymbol{x}) + g(\boldsymbol{x})\,\boldsymbol{u} \tag{6}$$

Other dynamic parameters (e.g., α and β) are treated as constants in the fast time scale since they evolve more slowly.

Each of the outputs of the fast time scale has a relative degree[1] of 1, and thus the total relative degree is 3. Since the total relative degree is equal to the number of states, this time scale will have no internal dynamics. The control law is given by Eq. (2), where the desired dynamics are chosen as commanded rotational accelerations:

$$\boldsymbol{v} = [\dot{p}_{sc} \quad \dot{q}_c \quad \dot{r}_{sc}]^T \tag{7}$$

The dynamics of the resulting closed-loop system (for the fast time scale) are governed by three decoupled integrators relating the rotational acceleration commands to their corresponding rotational rates.

The translational dynamics of the aircraft constitute the slow time scale for the aircraft control law design. Rotational accelerations are commanded to control the angle of attack and sideslip of the aircraft. The fast time scale states and controls are treated as constants in the slow time scale because of their faster evolution.

The states of the slow dynamics are given by

$$\boldsymbol{x} = [\alpha \quad \dot{\alpha} \quad \beta \quad \dot{\beta} \quad \phi \quad \theta \quad V \quad \dot{V}]^T \tag{8}$$

whereas the control inputs consist of the vehicle rotational accelerations,

$$\boldsymbol{u} = [\dot{p}_s \quad \dot{q} \quad \dot{r}_s]^T \tag{9}$$

The output vector contains the angle of attack and sideslip since these are the variables to be controlled. The output vector is augmented with the stability axis roll acceleration (corresponding to the trivial system $y = u$) to produce a square plant. The output vector is thus given by

$$\boldsymbol{y} = [\dot{p}_s \quad \alpha \quad \beta]^T \tag{10}$$

The dynamics of the slow time scale can be expressed in the form

$$\begin{bmatrix} \dot{\alpha} \\ \ddot{\alpha} \\ \dot{\beta} \\ \ddot{\beta} \\ \dot{\phi} \\ \dot{\theta} \\ \dot{V} \\ \ddot{V} \end{bmatrix} = \begin{bmatrix} f_4(\boldsymbol{x}) \\ f_5(\boldsymbol{x}) \\ f_6(\boldsymbol{x}) \\ f_7(\boldsymbol{x}) \\ f_8(\boldsymbol{x}) \\ f_9(\boldsymbol{x}) \\ f_{10}(\boldsymbol{x}) \\ f_{11}(\boldsymbol{x}) \end{bmatrix} + \begin{bmatrix} 0 & 0 & 0 \\ -\tan(\beta) & 1 & 0 \\ 0 & 0 & 0 \\ 0 & 0 & -1 \\ 0 & 0 & 0 \\ 0 & 0 & 0 \\ 0 & 0 & 0 \\ 0 & 0 & 0 \end{bmatrix} \begin{bmatrix} \dot{p}_s \\ \dot{q} \\ \dot{r}_s \end{bmatrix} \tag{11}$$

where $f_5(\boldsymbol{x})$, $f_7(\boldsymbol{x})$, $f_8(\boldsymbol{x})$, $f_9(\boldsymbol{x})$, and $f_{11}(\boldsymbol{x})$ are functions of the state vector, whereas the remaining functions consist of rows of zeros with a one in the appropriate location to equate the state derivative to its corresponding state. It follows that this system has a vector relative degree[1] of $\{0, 2, 2\}$ and thus a total relative degree of 4. Since the total relative degree is less than the number of states, internal dynamics will be present in this time scale.

The solution of the noninteracting controls problem yields a control law for the slow time scale as

$$\begin{bmatrix} \dot{p}_{sc} \\ \dot{q}_c \\ \dot{r}_{sc} \end{bmatrix} = \begin{bmatrix} 1 & 0 & 0 \\ -\tan(\beta) & 1 & 0 \\ 0 & 0 & -1 \end{bmatrix}^{-1} \left\{ \boldsymbol{v} - \begin{bmatrix} 0 \\ f_5(\boldsymbol{x}) \\ f_7(\boldsymbol{x}) \end{bmatrix} \right\} \tag{12}$$

The desired dynamics $\boldsymbol{v}$ of the slow time scale are selected based on flying qualities requirements.

Flying qualities requirements describe the aircraft response characteristics that pilots desire to complete various tasks. These guidelines have been developed through extensive research and are documented in Ref. 26. Flying qualities are ranked as level 1, 2, or 3. Level 1 indicates that flying qualities are clearly acceptable for the intended task. Level 2 indicates that flying qualities are adequate to complete a task, but improvements are desirable. Level 3 indicates that the aircraft is controllable, but the pilot workload is excessive and/or the mission effectiveness is inadequate.

In the longitudinal axis, flying qualities requirements can be specified in terms of a second-order angle of attack to longitudinal stick response, given by

$$\frac{\alpha}{\delta_{\text{LON}}} = \frac{K\omega_{\text{sp}}^2}{s^2 + 2\zeta_{\text{sp}}\omega_{\text{sp}}s + \omega_{\text{sp}}^2} \tag{13}$$

Requirements for the short period frequency ω_{sp} and damping ratio ζ_{sp} are given in terms of the vehicle lift curve slope, n_z/α. Lateral axis flying qualities are specified by the stability axis roll rate response to a lateral stick input. The desired first-order response is characterized by

$$\frac{p_s}{\delta_{\text{LAT}}} = \frac{K}{\tau_R s + 1} \tag{14}$$

Specifications for the roll mode time constant τ_R are given as a function of the maximum achievable steady-state roll rate. Directional axis flying qualities are specified in terms of the dutch roll frequency ω_d and damping ratio ζ_d. The desired second-order response characterizing the sideslip response to a directional control (pedal) input is given by

$$\frac{\beta}{\delta_{\text{DIR}}} = \frac{K\omega_d^2}{s^2 + 2\zeta_d\omega_d s + \omega_d^2} \tag{15}$$

The control law of Eq. (12) linearizes the angle of attack and sideslip responses of the aircraft but produces internal dynamics whose stability must be evaluated. Since the slow time scale dynamics are in normal form,[1] the states of the internal dynamics are directly identified as

$$\eta = [\phi \quad \theta \quad V \quad \dot{V}]^T \tag{16}$$

and thus consist of the phugoid and spiral modes of the aircraft. The phugoid mode is defined by changes in pitch attitude and velocity at a constant angle of attack, whereas the spiral mode is characterized by unconstrained roll motion at a constant sideslip angle. These modes are typically stabilized through feedback of attitudes, velocity, and accelerations. The stability of these modes is further augmented by the loop closure through the pilot.

Stability and Flying Qualities Robustness Tests

Modern control theory has yielded a variety of techniques for analyzing the robustness properties of control systems.[27] Most of these techniques require that the system be transformed to the $\Delta-M$ analysis model shown in Fig. 2. This model isolates the uncertain parameters in the block diagonal matrix Δ, whereas the transfer function matrix M represents the nominal closed-loop system, which is assumed stable. Models transformed to this structure can be used to assess both stability and performance robustness.

The $\Delta-M$ analysis model is commonly formed by using the signal flow graph decomposition technique described by Wise.[28] Uncertain parameters represented with a multiplicative uncertainty model are described by

$$p_i = p_{i0}(1 + \delta_i) \tag{17}$$

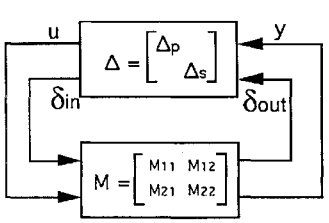

Fig. 2 $\Delta-M$ robustness analysis model.

where p_{i0} is the nominal parameter value and δ_i is the variation in the parameter. This uncertainty model is desirable since the parameter variations represent percentage deviations from the nominal values. This approach alleviates scaling problems introduced when evaluating robustness with parameters having greatly different magnitudes and units (e.g., velocity and stability derivatives). If desired, weights can be added to the individual parameter variations,

$$p_i = p_{i0}(1 + w_i\delta_i) \tag{18}$$

to scale the relative variations of the parameters. This approach can be used to refine robustness bounds if one has a priori knowledge that certain parameters are known more accurately than others and thus can vary less.

The multiplicative uncertainty model cannot be used when parameters have a nominal value of zero since the percentage variation δ_i does not change the parameter from its nominal value. In this case, an additive uncertainty model can be used where the uncertain parameter is given by

$$p_i = p_{i0} + w_i\delta_i \tag{19}$$

With this model, the parameter uncertainties represent changes in the numerical value of the parameter.

When evaluating robust stability, the Δ matrix contains the uncertain parameters. The goal of the robustness test is to bound the simultaneous parameter variations that can be tolerated while maintaining stability. This equates to determining the maximum simultaneous parameter variations, in the worst case directions, for which the system remains stable. The foundation of tests for bounding the parameter variations lies in the multivariable Nyquist theorem[29] and the fact that the closed-loop characteristic polynomial (poles) of the perturbed system $\phi'_{\text{CL}}(s)$ is related to that of the nominal system $\phi_{\text{CL}}(s)$ by

$$\phi'_{\text{CL}}(s) = \phi_{\text{CL}}(s) \cdot \det[I - \Delta M] \tag{20}$$

It is easy to see that when $\Delta = 0$ (no uncertainty), $\phi'_{\text{CL}}(s) = \phi_{\text{CL}}(s)$. If the nominal closed-loop system is stable, instability can occur in the perturbed system only if $\det[I - \Delta M]$ introduces an additional encirclement of the critical point in the complex plane. This change in the number of encirclements can only occur when the $\det[I-\Delta M]$ is singular, i.e., $\det[I - \Delta M] = 0$. As a result, the stability robustness tests aim to bound the parameter variations by determining the smallest set of uncertain parameters for which $\det[I - \Delta M]$ is singular.

Wise[27] compared several of the techniques for assessing the stability robustness of a missile autopilot design to uncertain aerodynamic parameters. The deGaston–Safonov real multiloop stability margin[20] produced exact bounds and was verified by Monte Carlo eigenanalysis. The SSV μ (Ref. 21) produced a more conservative result, partially because of the use of the complex μ algorithm for assessing robustness to real parameter variations. The complex μ algorithm models the real parameter uncertainty as a complex disk (arbitrary phase) and determines the smallest radius of this disk that makes the return difference matrix, $I-\Delta M$, singular. Modeling real parameter variations (like aerostability derivatives) with a complex disk leads to conservative results.

The SSV μ bounds the variations in the uncertain parameters through an algorithm that uses diagonal scaling of the Δ matrix to determine the worst case direction for parameter variations. The worst case direction corresponds to the smallest set of destabilizing parameters.

The deGaston–Safonov real multiloop stability margin bounds the allowable parameter variations by mapping the space of uncertain parameters into the complex plane using the multivariable Nyquist theorem. The algorithm is illustrated in Fig. 3 for the case of three uncertain parameters. The hypercube on the left-hand side represents the allowable variations in the three uncertain parameters (Δ), with the origin corresponding to the nominal set of parameters. If the parameter space was mapped directly into the complex plane through $\det[I - \Delta M]$, it would create the shaded region in Fig. 3.

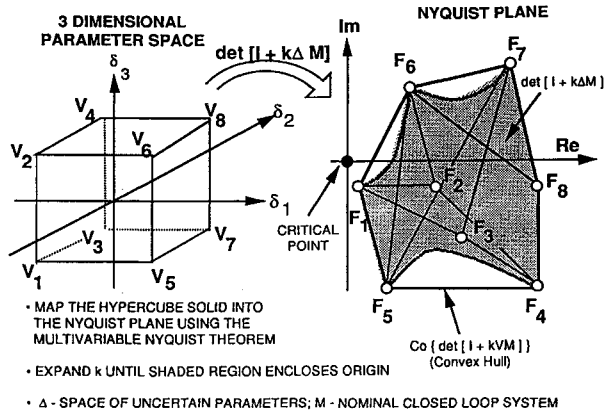

Fig. 3 DeGaston–Safonov real multiloop stability margin algorithm.

This procedure is computationally unrealistic since an infinite number of points would have to be mapped. The deGaston–Safonov algorithm instead maps the vertices of the parameter space hypercube into the complex plane and forms a convex hull using the mapped points. This convex hull encloses the image of the parameter space hypercube mapped in the complex plane, as shown. Enlarging the parameter space hypercube until the convex hull encircles the critical point (origin) in the complex plane provides a lower bound on the allowable parameter variations. If the set of destabilizing parameters lies on the edge of the parameter space hypercube, the lower bound defines the exact robustness bound.

Both of the robustness analysis techniques have advantages and disadvantages. The obvious advantage of the deGaston–Safonov real multiloop stability margin is its ability to provide the exact robustness bound. It is somewhat limited in that it can only handle real parameter variations (i.e., cannot assess robustness to complex parameters such as time delays). In addition, it is limited in the number of simultaneous parameter variations that it can assess by the computational requirements. The SSV μ approach is more computationally efficient and can handle a larger number of simultaneous, as well as complex, parameter variations, but it produces results that may be conservative. The SSV μ technique can also be used to assess robust performance. These evaluations are intended to identify the parameter variations that can be tolerated while maintaining stability and meeting a specified performance criterion (flying qualities, disturbance rejection, ...).

The robust stability tests discussed earlier determine the set of parameter variations that bound the "size" of the matrix Δ. Typically, robust performance requirements cannot be described by bounding the same Δ used to analyze robust stability. A performance objective may be that a frequency response $f(j\omega)$ lie below some bound $b(j\omega)$, i.e., $|f(j\omega)| < |b(j\omega)|$. This requirement can be equivalently formulated as

$$|f(j\omega)b^{-1}(j\omega)| < 1 \tag{21}$$

where $b^{-1}(j\omega)$ is referred to as the performance weighting filter. Using Eq. (21), it follows that $f(j\omega)b^{-1}(j\omega)$ can be bounded by a complex disk. This reformulation makes the performance requirement "look" like the stability requirement and allows it to be cast into the Δ–M analysis model structure.

The Δ–M analysis model supports both stability and performance robustness when the Δ matrix is partitioned to contain a robust performance requirement Δ_p and a robust stability requirement Δ_s as

$$\Delta = \begin{bmatrix} \Delta_p & 0 \\ 0 & \Delta_s \end{bmatrix} \tag{22}$$

The transfer function matrix M is partitioned in a corresponding manner as

$$M = \begin{bmatrix} M_{11} & M_{12} \\ M_{21} & M_{22} \end{bmatrix} \tag{23}$$

Using SSV μ analysis, the necessary and sufficient conditions for stability and performance robustness are[30]

$$\left\| \left[M_{11} + M_{12}\Delta_s(I - M_{22}\Delta_s)^{-1}M_{21} \right] \Delta_p \right|_\infty < 1$$
$$|M_{22}|_\mu < 1 \tag{24}$$

where $|\cdot|_\infty$ represents the infinity norm and $|\cdot|_\mu$ represents the SSV μ bound. These conditions are guaranteed if

$$\bar{\sigma}[\Delta] < \frac{1}{\max_\omega |M|_\mu} \tag{25}$$

As a result, computing the SSV μ bound of M defines the maximum size of Δ and thus bounds the parameter variations that satisfy both the stability and performance robustness constraints.

Recent studies published in the literature[22] have analyzed flying qualities robustness by determining the minimum parameter variations that cause a closed-loop flight control system to violate the Bode mismatch envelopes relative to the desired low-order response characteristics. The Bode mismatch envelopes, shown in Fig. 4, are commonly used to verify that a low-order equivalent model adequately captures the dynamics of a high-order response and thus may be used to validate a design against the Military Standard 1797A[26] flying qualities requirements. The Bode mismatch envelopes bound the allowable magnitude and phase variations, relative to the desired low-order response, which are unnoticeable to the pilot. If the difference between the low- and high-order frequency responses falls within the Bode mismatch envelope, the pilot will sense the desired low-order response.

The premise behind the flying qualities robustness measure of Anderson[22] is that parameter variations, which cause the difference between the high-order and desired low-order responses to violate the Bode mismatch envelope, will be noticeable to the pilot and hence will degrade flying qualities. A robustness analysis test is established to bound the parameter variations so that changes in the aircraft dynamics will not be detected by the pilot. The frequency response employed by this robustness test is the difference between the perturbed high-order system and the nominal low-order system (desired flying qualities model). A performance weighting filter, derived from the Bode mismatch envelope, processes this signal to form the robust performance criterion. Anderson derives this weighting filter using inequalities involving the upper and lower magnitude bounds of the Bode mismatch envelopes. An alternate derivation is provided here that highlights both the magnitude and phase bounds implied by the robustness test.

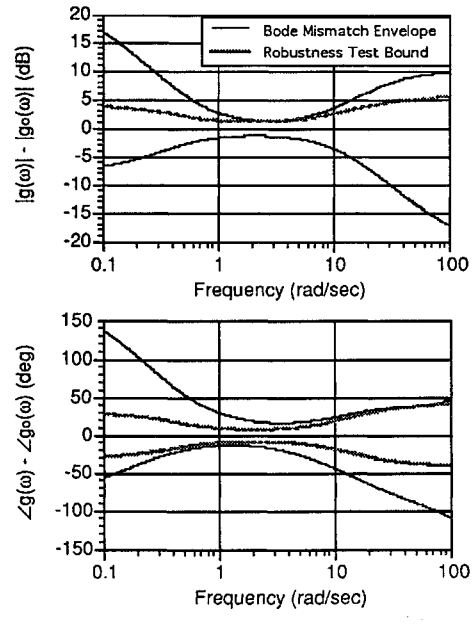

Fig. 4 Bode mismatch envelope.

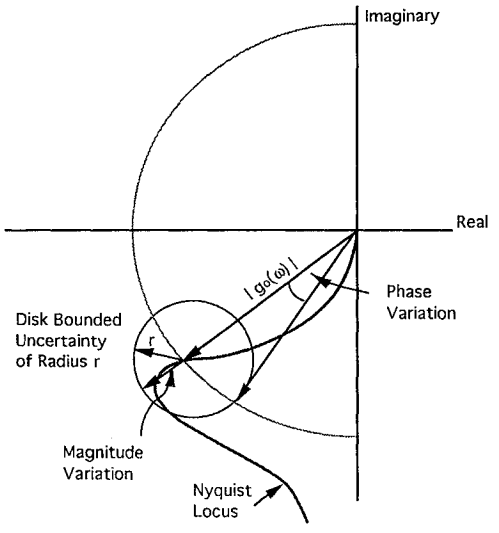

Fig. 5 Nyquist diagram for derivation of performance weighting filter.

The Bode mismatch envelopes bound the magnitude (decibels) and phase variations between the high- and low-order system responses as

$$|m_L(\omega|_{\text{dB}} < |g(\omega)|_{\text{dB}} - |g_0(\omega)|_{\text{dB}} < |m_U(\omega)|_{\text{dB}} \tag{26}$$

$$\angle m_L(\omega) < \angle g(\omega) - \angle g_0(\omega) < \angle m_U(\omega) \tag{27}$$

where $m_L(\omega)$ represents the lower bound of the Bode mismatch envelope (decibels), $m_U(\omega)$ represents the upper bound of the Bode mismatch envelope (decibels), $g_0(\omega)$ represents the nominal or low-order system (desired flying qualities), and $g(\omega)$ is the perturbed high-order system. To determine the required weighting filter, we must examine how the gain and phase variations of the Bode mismatch envelopes are related to a disk bounded uncertainty.

Consider the Nyquist plot of the nominal system shown in Fig. 5. At a given frequency, the Nyquist locus is described by a magnitude and phase angle, which is represented by the vector of length $|g_0(\omega)|$ centered at the origin pointing to the Nyquist locus. Magnitude variations in the loop transfer function alter the length of the vector along its nominal direction, whereas phase variations cause a rotation of the vector. The disk bounded uncertainty under consideration is represented by a circle of radius r centered at the point on the nominal Nyquist locus. We would like to determine the radius of this disk, which guarantees that the Bode mismatch envelope magnitude and phase constraints remain satisfied. The SSV μ test can then be used to bound the parameter variations such that the loop gain is restricted to this disk, thus guaranteeing robust performance for the Bode mismatch envelope criterion.

To guarantee robust performance with the disk bounded uncertainty, we must select the most conservative disk radius that satisfies the magnitude and phase variation bounds from the Bode mismatch envelopes. The radius required to satisfy each of the criteria may be directly computed from the Bode mismatch envelopes. The minimum radius is then used as the performance requirement that guarantees that all criteria are met. Using Figs. 4 and 5, the disk radius required for each criterion is found to be as follows.

Upper magnitude bound:

$$r_{|m_U(\omega)|} = 10^{|m_U(\omega)|/20} - 1$$

Lower magnitude bound:

$$r_{|m_L(\omega)|} = 1 - 10^{|m_L(\omega)|/20}$$

Upper phase bound:

$$r_{\angle m_U(\omega)} = \tan[\angle m_U(\omega)]$$

Lower phase bound:

$$r_{\angle m_L(\omega)} = -\tan[\angle m_L(\omega)] \tag{28}$$

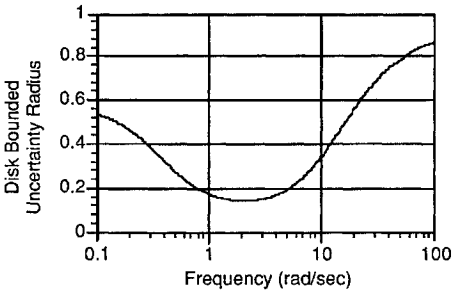

Fig. 6 Disk bounded uncertainty radius for flying qualities robustness test.

These requirements on the disk radius only depend on the Bode mismatch envelopes and are not a function of the nominal loop gain and phase. The disk radius is shown as a function of frequency in Fig. 6. This figure indicates that the allowable gain and phase variations are smallest in the pilot's primary frequency range (1–10 rad/s), which correlates with the Bode mismatch envelopes.

The disk bounded uncertainty radius implies an allowable magnitude and phase variation at each frequency by the inverse of the relationships in Eq. (28). These allowable gain and phase variations are compared with the Bode mismatch envelopes in Fig. 4. The comparison shows that the lower magnitude bound of the Bode mismatch envelopes is the constraint that defines the disk bounded uncertainty radius of Fig. 6. The robustness test is thus conservative in evaluating robust performance to the upper magnitude bound and phase angle criteria as shown in the robustness bounds of Fig. 4.

The disk bounded uncertainty radius of Fig. 6 specifies the maximum amount that the gain of the perturbed system can deviate from that of the nominal system. This is expressed mathematically (considering it as a gain increase) as

$$\frac{|g(\omega)|}{|g_0(\omega)|} - 1 < r \tag{29}$$

This, in turn, implies

$$\frac{|g(\omega)| - |g_0(\omega)|}{|g_0(\omega)|r} < 1 \tag{30}$$

Using the triangle inequality,

$$\frac{|g(\omega) - g_0(\omega)|}{|g_0(\omega)|r} \le \frac{|g(\omega)| - |g_0(\omega)|}{|g_0(\omega)|r} < 1 \tag{31}$$

and the robustness test becomes

$$\frac{|g(\omega) - g_0(\omega)|}{|g_0(\omega)|r} \le |g(\omega) - g_0(\omega)|W(s) < 1 \tag{32}$$

In Eq. (32), $W(s)$ represents the performance weighting filter. For implementation purposes, it is desirable to have the disk bounded uncertainty radius expressed as a transfer function. A second-order transfer function was fit to the data of Fig. 6, yielding

$$r = \left| \frac{s^2 + 4.1s + 4.4}{1.17s^2 + 29.63s + 7.33} \right| \tag{33}$$

which agrees with the result derived by Anderson.[22] Using Eqs. (32) and (33), one can compute the weighting filter required to assess flying qualities robustness. Robust flying qualities measured by the Bode mismatch envelopes may then be assessed using the SSV μ test as discussed earlier.

The stability and performance robustness bounds are a function of frequency. The minimum bound over all frequencies defines the parameter variations that can be tolerated while satisfying the specified stability and performance criteria.

It is common practice to evaluate robust stability at nonzero frequencies covering the control bandwidth (see Wise[27] and the references therein). Analysis results indicate that the robustness bound at dc can limit the allowable parameter variations. The robustness bound at dc defines the amount that the uncertain parameters can

vary before introducing a sign change in the constant term of the closed-loop characteristic polynomial. The dc bound has been found to limit the allowable parameter variations for statically stable vehicles and is evaluated as part of this analysis.

The robustness bound at dc can be independent of the control law's feedback gains for some control law structures. Consider the closed-loop characteristic equation given by

$$s^n + \alpha_{n-1}s^{n-1} + \cdots + \alpha_0 = 0 \tag{34}$$

If the constant term α_0 is a function of the uncertain parameters, a sign change in this term defines the dc robustness bound. If the feedback gains do not enter into this term in an affine way, they will not impact the robustness bound. If this is the case, the dc robustness bound can only be improved by modifying the aircraft surface mixer (Fig. 1). The surface mixer alters the zeros of the system. When the loops are closed via feedback, the surface mixer alters how uncertain parameters, such as the aerodynamic stability derivatives, enter into α_0. In Wise,[31] surface mixing logic was designed to reduce induced roll-yaw coupling. Modifying the surface mixing logic may be a way to improve the robustness properties of aircraft control laws designed using feedback linearization.

Robustness Analysis

The feedback linearization based control law investigated in this paper was evaluated based on stability and flying qualities robustness to aerodynamic parameter uncertainties. This evaluation was conducted for both the longitudinal and lateral directional axes at the extremes (corners) of the flight envelope [high and low Mach and high and low angle of attack (AOA)]. All uncertain parameters were represented with a multiplicative uncertainty model and were equally weighted.

The stability and flying qualities robustness tests utilize the $\Delta - M$ interconnection structure, which was generated from the model shown in Fig. 7. This model consists of the rigid-body dynamics and controller linearized around a trim operating point. Digitization effects and higher-order dynamics are included to ensure realistic performance predictions. A pilot stabilization model was included to augment the stability of the phugoid and spiral modes via attitude feedback, since a nominally stable system is required to implement the robustness tests. Alternative methods for analyzing the robustness of systems having unstable phugoid and spiral modes have been proposed by Miotto and Paduano.[32] The flying qualities dynamics model and performance weighting filter describe the performance requirement for the robust flying qualities evaluation. The resulting Δ matrix contains both stability Δ_s and performance Δ_p uncertainties and is described by

$$\begin{bmatrix} \boldsymbol{u} \\ \delta_i \end{bmatrix} = \Delta \begin{bmatrix} \boldsymbol{y} \\ \delta_o \end{bmatrix} = \begin{bmatrix} \Delta_p & 0 \\ 0 & \Delta_s \end{bmatrix} \begin{bmatrix} \boldsymbol{y} \\ \delta_o \end{bmatrix} \tag{35}$$

Robust stability ($\Delta_p = 0$) was evaluated using the deGaston–Safonov real multiloop stability margin.[20] Both dc and nonzero frequencies were considered. SSV μ (Ref. 21) analysis was used to evaluate flying qualities robustness ($\Delta_p \neq 0$) using a performance weighting filter based on the Bode mismatch envelope and given by Eqs. (32) and (33). Flying qualities robustness was evaluated at nonzero frequencies where the Bode mismatch envelopes are defined. In each case, the robustness bound was first computed at a specified set of frequencies. At each dip in the robustness bound, a conjugate gradient algorithm was then initiated to refine each local minima.

Implementation of the flying qualities robustness test was accomplished using the model of Fig. 7. For the longitudinal axis, the input $\boldsymbol{u}$ represents the pilot's longitudinal stick deflection, whereas the flying qualities dynamics model represents the desired angle of attack to longitudinal stick response characteristic. Note that the pitch rate response could alternatively be used. For the lateral directional axis, the input $\boldsymbol{u}$ is a vector composed of the pilot's lateral stick and rudder pedal deflections. The flying qualities dynamics model is a transfer function matrix containing the desired roll rate to lateral stick and sideslip to rudder pedal responses. The performance weighting filter is also a transfer function matrix containing the appropriate performance weighting transfer functions for each response.

The stability and flying qualities robustness of the feedback linearization control law was evaluated using a set of uncertain parameters consisting of the primary short period aerodynamic stability derivatives. The robustness analysis results are summarized in Table 1. These data indicate that the robust stability of the system is limited by the dc robustness bound at most of the flight conditions analyzed. When the robust stability bound occurs at dc, the bound is exact. Good stability and flying qualities robustness was observed in the pitch axis for all flight conditions, whereas the roll-yaw axis was found to be sensitive to the parameter uncertainties.

Table 1 Stability and flying qualities robustness results

Uncertain parameters	Pitch $C_{X\alpha}, C_{Z\alpha}, C_{m\alpha}$ $C_{X\delta}, C_{Z\delta}, C_{m\delta}$		Roll yaw $C_{Y\beta}, C_{l\beta}, C_{n\beta}$ $C_{Y\delta}, C_{l\delta}, C_{n\delta}$	
Robustness bounds	dc	non-dc	dc	non-dc
Stability robustness				
Low speed, low AOA	0.66	0.64	0.50	0.53
Low speed, high AOA	0.41	0.54	0.11	0.46
High speed, low AOA	0.29	0.45	0.17	0.23
High speed, high AOA	0.44	0.50	0.50	0.47
Flying qualities robustness				
Low speed, low AOA	—	0.27	—	0.06
Low speed, high AOA	—	0.29	—	0.06
High speed, low AOA	—	0.16	—	0.06
High speed, high AOA	—	0.17	—	0.06

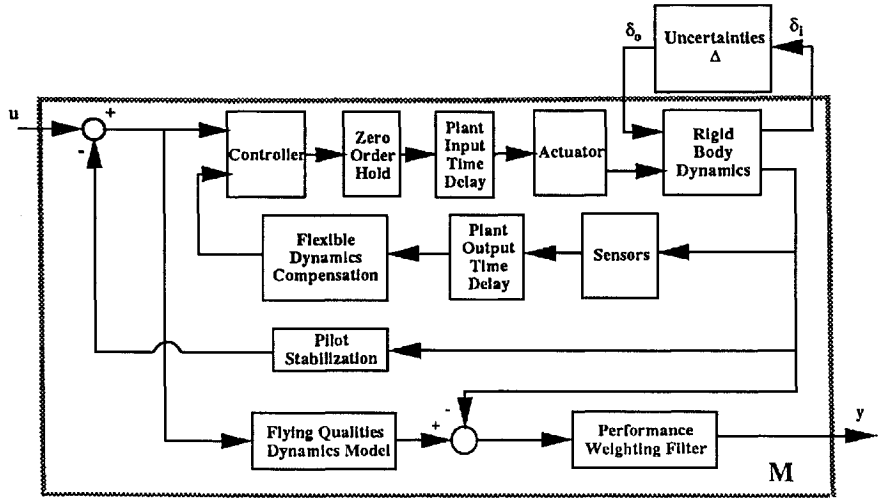

Fig. 7 Robustness analysis model.

Plots of the stability and flying robustness bounds are shown for the pitch and roll-yaw planes at the high-speed, low-AOA flight condition in Figs. 8–11. The dc robustness bound is indicated by an open circle on the stability robustness curves.

In addition to the dc bound, the stability robustness curves also exhibit local minima near the gain and/or phase crossover frequencies. This result agrees with intuition since these are the frequencies at which classical stability margins are defined. Gain or phase variations induced by the uncertain parameters at these frequencies directly reduce the stability margins. At high frequencies, the small parameter variations may produce a phase crossover, but large parameter variations are required to produce a destabilizing loop gain. As a result, the robustness bounds increase at high frequencies.

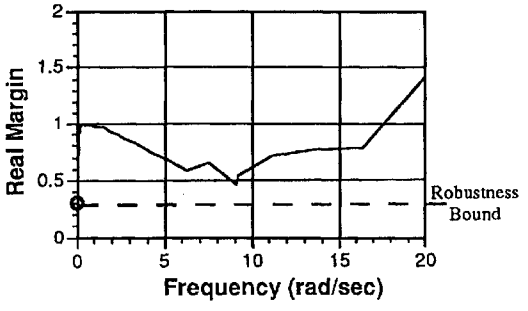

Fig. 8 Stability robustness bound: longitudinal axis, high speed, and low AOA.

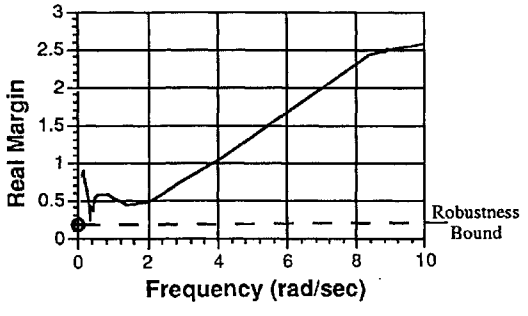

Fig. 9 Stability robustness bound: lateral directional axis, high speed, and low AOA.

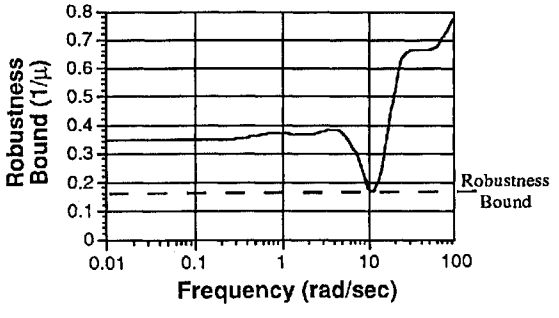

Fig. 10 Flying qualities robustness bound: longitudinal axis, high speed, and low AOA.

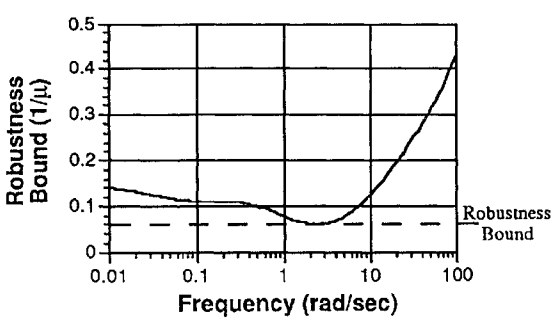

Fig. 11 Flying qualities robustness bound: lateral directional axis, high speed, and low AOA.

The shape of the performance robustness bound vs frequency curve is strongly influenced by the performance criterion under evaluation [weighting filter $W(s)$]. Since the Bode mismatch envelope imposes the most stringent requirement in the pilot's critical frequency range (1–10 rad/s), it is reasonable to expect that the minimum flying qualities robustness bound will occur in this region. Figures 10 and 11 indicate that this is the case for both the pitch and roll-yaw axes.

Conclusions

Aircraft control laws based on feedback linearization offer several advantages over other approaches. This approach enables direct incorporation of flying qualities objectives in the design process and can address the nonlinearities introduced by innovative control effectors and aircraft operation at extreme flight conditions. The primary disadvantage of this control design approach is the dependence on knowing the aircraft's aerodynamic stability derivatives and the lack of robustness guarantees for the closed-loop system.

The analysis methods presented used linearized models of the aircraft dynamics and nonlinear control laws designed using feedback linearization. For these linear analysis models, the real multiloop stability margin and the structured singular value offer two methods for evaluating robust stability and robust performance. The real margin results indicated that the robust stability bounds were exact stability bounds and that the aircraft could only tolerate as little as 11% variation in its stability derivatives before going unstable (derived from the lateral directional model). The structured singular value analysis evaluating robust performance produced parameter variation bounds smaller than the robust stability bounds generated by the real margin. This was expected since the robust performance analysis model includes the robust stability uncertainties. The lateral directional flying qualities were found to be very sensitive, with a 6% allowable parameter variation before the Bode mismatch envelope would be violated.

References

[1]Isidori, A., *Nonlinear Control Systems*, 2nd ed., Springer–Verlag, New York, 1989.

[2]Vidyasager, M., *Nonlinear Systems Analysis*, 2nd ed., Prentice–Hall, Englewood Cliffs, NJ, 1993.

[3]Bugajski, D. J., Enns, D. F., and Elgersma, M. R., "A Dynamic Inversion Based Control Law with Application to the High Angle-of-Attack Research Vehicle," *Proceedings of the AIAA Guidance, Navigation, and Control Conference* (Portland, OR), AIAA, Washington, DC, 1990, pp. 826–839.

[4]Snell, S. A., Enns, D. F., and Garrard, W. L., Jr., "Nonlinear Inversion Flight Control for a Supermaneuverable Aircraft," *Proceedings of the AIAA Guidance, Navigation, and Control Conference* (Portland, OR), AIAA, Washington, DC, 1990, pp. 808–825.

[5]Morton, B., "A Dynamic Inversion Control Approach for High-Mach Trajectory Tracking," *Proceedings of the American Control Conference* (Chicago, IL), American Automatic Control Council, Baltimore, MD, 1992, pp. 1332–1336.

[6]Snell, A., "Cancellation Control Law for Lateral-Directional Dynamics of a Supermaneuverable Aircraft," *Proceedings of the AIAA Guidance, Navigation, and Control Conference* (Monterey, CA), AIAA, Washington, DC, 1993, pp. 701–709.

[7]Anon., "Multivariable Control Design Guidelines," First Draft, Honeywell Technology Center, Minneapolis, MN (for Air Force), May 1995.

[8]Wise, K. A., Dierks, M. W., Kerkemeyer, B., and Tang, J., "Linear and Nonlinear Aircraft Flight Control for the AIAA Controls Design Challenge," AIAA Paper 92-4628, Aug. 1992.

[9]Buffington, J. M., Adams, R. J., and Banda, S. S., "Robust, Nonlinear, High Angle-of-Attack Control Design for a Supermaneuverable Vehicle," *Proceedings of the AIAA Guidance, Navigation, and Control Conference* (Monterey, CA), AIAA, Washington, DC, 1993, pp. 690–700.

[10]Reiner, J., Balas, G. J., and Garrard, W. L., "Robust Dynamic Inversion for Control of Highly Maneuverable Aircraft," *Journal of Guidance, Control, and Dynamics*, Vol. 18, No. 1, 1995, pp. 18–24.

[11]Safonov, M., Goh, K., and Ly, J., "Control System Synthesis via Bilinear Matrix Inequalities," *Proceedings of the American Control Conference*, American Automatic Control Council, Baltimore, MD, 1994, pp. 45–49.

[12]Goh, K., Ly, J., Safonov, M., Papavassilopoulis, G., and Turan, L., "Biaffine Matrix Inequality Properties and Computation Methods," *Proceedings of the American Control Conference*, American Automatic Control Council, Baltimore, MD, 1994, pp. 850–855.

[13]Akhrif, O., and Blankenship, G. L., "Robust Stabilization of Feedback Linearizable Systems," *Proceedings of the IEEE Conference on Decision and Control* (Austin, TX), 1988, pp. 1714–1719.

[14]Snell, S. A., "Preliminary Assessment of the Robustness of Dynamic Inversion Based Flight Control Laws," *Proceedings of the AIAA Guidance, Navigation, and Control Conference* (Hilton Head, SC), AIAA, Washington, DC, 1992, pp. 206–216.

[15]Schoenwald, D. A., and Ozguner, U., "Robust Feedback Linearization of Uncertain Nonlinear Systems," *Proceedings of the American Control Conference* (Chicago, IL), American Automatic Control Council, Baltimore, MD, 1992, pp. 2545, 2546.

[16]Tierno, J., and Murray, R., "Robust Performance Analysis for a Class of Uncertain Nonlinear Systems," *Proceedings of the 34th IEEE Conference on Decision and Control* (New Orleans, LA), 1995, pp. 1684–1689.

[17]Tierno, J., Murray, R., Doyle, J., and Gregory, I., "Numerically Efficient Robustness Analysis of Trajectory Tracking for Nonlinear Systems," *Journal of Guidance, Control, and Dynamics* (submitted for publication).

[18]Enns, D., "Robustness of Dynamic Inversion vs μ Synthesis: Lateral-Directional Flight Control Example," *Proceedings of the AIAA Guidance, Navigation, and Control Conference* (Portland, OR), AIAA, Washington, DC, 1990, pp. 210–222.

[19]Balas, G. J., Garrard, W. L., and Reiner, J., "Robust Dynamic Inversion Control Laws for Aircraft Control," *Proceedings of the AIAA Guidance, Navigation, and Control Conference* (Hilton Head, SC), AIAA, Washington, DC, 1992, pp. 192–205.

[20]DeGaston, R. R. E., and Safonov, M. G., "Exact Calculation of the Multiloop Stability Margin," *IEEE Transactions on Automatic Control*, Vol. 33, No. 2, 1988, pp. 156–171.

[21]Doyle, J. C., "Analysis of Feedback Systems with Structured Uncertainties," *IEEE Proceedings*, Vol. 129, Pt. D, No. 6, 1982, pp. 242–250.

[22]Anderson, M. R., "Robustness Evaluation of a Flexible Aircraft Control System," *Proceedings of the AIAA Guidance, Navigation, and Control Conference* (Portland, OR), AIAA, Washington, DC, 1990, pp. 1170–1179.

[23]McGruer, D., Ashkenas, I., and Graham, D., *Aircraft Dynamics and Automatic Control*, Princeton Univ. Press, Princeton, NJ, 1973.

[24]Blakelock, J. H., *Automatic Control of Aircraft and Missiles*, 2nd ed., Wiley, New York, 1991.

[25]Wise, K. A., and Broy, D. J., "Agile Missile Dynamics and Control," AIAA Paper 96-3912, July 1996.

[26]Anon., "Military Standard, Flying Qualities of Piloted Vehicles," MIL-STD-1797A, U.S. Air Force, Jan. 1990.

[27]Wise, K. A., "A Comparison of Six Robustness Tests for Evaluating Missile Autopilot Uncertainties," *Journal of Guidance, Control, and Dynamics*, Vol. 15, No. 4, 1992, pp. 861–870.

[28]Wise, K. A., "A Parameter Space Robustness Test for Real and Complex Uncertainties," *Proceedings of the 32nd IEEE Conference on Decision and Control* (San Antonio, TX), 1993, pp. 2486–2492.

[29]MacFarlane, A. G. J., *Frequency-Response Methods in Control Systems*, Inst. of Electrical and Electronics Engineers, New York, 1979.

[30]Maciejowski, J. M., *Multivariable Feedback Design*, Addison–Wesley, New York, 1989.

[31]Wise, K. A., "Optimizing Singular Value Robustness Measures in a Conventional Bank-to-Turn Missile Autopilot Design," *Proceedings of the AIAA Guidance, Navigation, and Control Conference* (Minneapolis, MN), AIAA, Washington, DC, 1988, pp. 296–306.

[32]Miotto, P., and Paduano, J., "Application of Real Structured Singular Values to Flight Control Validation Issues," *Proceedings of the AIAA Guidance, Navigation, and Control Conference* (Baltimore, MD), AIAA, Washington, DC, 1995, pp. 151–163.